Optics Letters

Arbitrarily directed emission of integrated cylindrical vector vortex beams by geometric phase engineering

YOEL SEBBAG AND **URIEL LEVY***

Department of Applied Physics, the Faculty of Science, the Center for Nanoscience and Nanotechnology, the Hebrew University of Jerusalem, Jerusalem 91904, Israel
**Corresponding author: ulevy@mail.huji.ac.il*

Received 9 October 2020; revised 19 November 2020; accepted 19 November 2020; posted 20 November 2020 (Doc. ID 412026); published 14 December 2020

Integrated cylindrical vector vortex (CVV) emitters have been introduced and studied for their potential applications in classical optics and quantum optics technologies. In this work, we demonstrate that the emission angle of integrated CVV emitters can be engineered by taking advantage of the geometrical phase of a microring resonator. Two methods to superimpose an arbitrary phase profile on top of the integrated emitters are presented and compared. Angled emission of integrated vector vortex beams enables the use of chip-scale emitters for integrated nonlinear optics and for beam steering applications with orbital angular momentum.

https://doi.org/10.1364/OL.412026

Cylindrical vector vortex (CVV) beams carry simultaneously spin and orbital angular momentum (OAM). Spin angular momentum (SAM) is the property of light that is associated with its polarization, while OAM is a degree of freedom that is associated with helical waveform, with topological charge, generally denoted by the integer l. When solving Maxwell's equations in cylindrical coordinates, l is associated to the azimuthal phase $\exp(il\phi)$. CVV beams have been used in a wide range of applications, including in microscopy [1], optical tweezers [2], optical trapping [3], and precision measurements [4].

Recently, OAM has gained significant attention due to its inherent properties. The unlimited topological charges and their orthogonality may provide a tremendous resource for increasing the channel capacity in classical telecommunication systems [5]. Moreover, the high-dimensional states provided by OAM show great potential for quantum communication [6], quantum information processing [7], and quantum computation [8].

Driven by the attractiveness of developing compact, robust, and complex integrated circuits that incorporate OAM, on-chip CVV emitters based on microring resonators have been demonstrated and widely investigated [9–16]. On top of the obvious advantages provided by such integration, on-chip emitters enable development of active devices [12], and engineering of the state of polarization (SoP) of the emitted CVV beam [13,14].

While the emission of vector vortex beams to free space has been mainly considered for data transmission and linear interactions, its use for nonlinear interactions remains challenging, yet highly desired. For example, generation of on-demand single photons at room temperature was recently demonstrated, using four-wave mixing in a sub-micrometer atomic vapor cell [17]. Moreover, conservation of total OAM in four-wave mixing enables efficient transfer of OAM to the generated light [18]. Thus, using CVV emitters for nonlinear interactions in an atomic-nanophotonic chip [19,20] can lead toward development of integrated single photon sources with engineered SoP.

CVV emitters based on microring resonators use an angular grating embedded in the inner sidewall of the ring to couple the whispering gallery mode (WGM) of the microring to a CVV mode that radiates perpendicular to the plane of the microring. However, efficient nonlinear interactions require phase matching, which is generally achieved by tuning the angle of the interacting beams in the nonlinear material.

Here we propose and compare two methods to generate CVV beams propagating at a specific angle with respect to the axis normal of the ring surface, by taking advantage of the geometrical phase of the propagating wave in the microring resonator. While the first method is straightforward and easy to implement, the other one presents an important feature, as it preserves the ability to tailor the SoP of the emitted vector vortex beam.

Generally speaking, the angular grating embedded in the microring resonator acts as a second-order grating, in which the WGM is scattered out of plane by the grating elements. In the small perturbation regime, each grating element can be approximated as a radiating dipole, with a polarization defined by the local optical field being scattered [13–15]. The SoP of the emitted CVV beams is determined by the collective interference of these radiative dipoles, and it can be engineered by tailoring the geometrical dimensions of the microring waveguide [13]. Constructive interference occurs when the angular phase matching condition is satisfied,

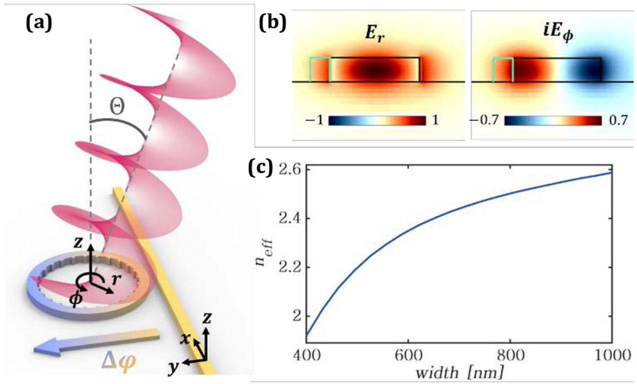

Fig. 1. (a) Sketch of slant emission of CVV beam by superimposing a linear phase onto the ring emitter. (b) Radial and azimuthal field components of the fundamental TE mode of a silicon waveguide with 3.9 μm radius, 450 nm width, and 180 nm height, at a wavelength of 1.55 μm. (c) Effective refractive index of the fundamental TE mode as a function of the waveguide width, assuming a curved waveguide with bending radius of 3.9 μm.

$$l = p - g * q, \qquad (1)$$

where l is the topological charge of the emitted beam, p is the WGM mode order, g is an integer, and q is the number of grating elements. The latter is related to the grating period, Λ_0, by $q = 2\pi R/\Lambda_0$, where R is the radius of the microring resonator.

Emitting CVV beams at an angle with respect to out of plane normal axis requires us to superimpose a linear global phase, $\Delta\varphi$, to the ring resonator in a Cartesian direction, as illustrated in Fig. 1(a). This phase can be implemented on the ring by using two different methods. In the first approach, the linear phase is obtained by varying the width of the ring waveguide, while keeping the separation between the grating elements (Λ_0) constant. Since the effective index of the propagating mode, n_{eff}, depends on the geometry of the waveguide [Fig. 1(c)], the optical phase accumulated between two equally separated scattering elements varies as function of the azimuthal coordinate, and it can be written as $\delta\varphi = \frac{2\pi R}{\lambda}\int_{\phi_i}^{\phi_i+\Delta\phi} n_{\text{eff}}(\theta)\mathrm{d}\theta$, where λ is the wavelength of the light and ϕ_i is the azimuthal coordinate of the ith grating element. Thus, a global phase can be implemented by tuning the width of the waveguide between each element.

To demonstrate the ability to tune the emission angle of the CVV emitters, we use 3D finite-difference-time-domain (FDTD) solver (Lumerical). In order to limit the computation time to a realistic value, we simulate fairly small silicon microring resonators at telecom wavelength, about 1550 nm. The high index contrast of silicon enables operating ring radii down to 3 μm, which simplifies the FDTD calculations.

In order to demonstrate the ability to emit CVV beams at an angle with respect to the z axis [Fig. 1(a)] by tuning the width of the ring's waveguide, we simulate a silicon microring resonator with a radius of 3.9 μm, a waveguide width of 450 nm, and a height of 180 nm, with 33 grating elements. The cross-sectional electric field distribution of the fundamental TE mode is presented in Fig. 1(b), showing the radial component E_r and the azimuthal one iE_ϕ. The scattered field is highlighted as a green box. The effective refractive index of the mode as function of the waveguide width is presented in Fig. 1(c).

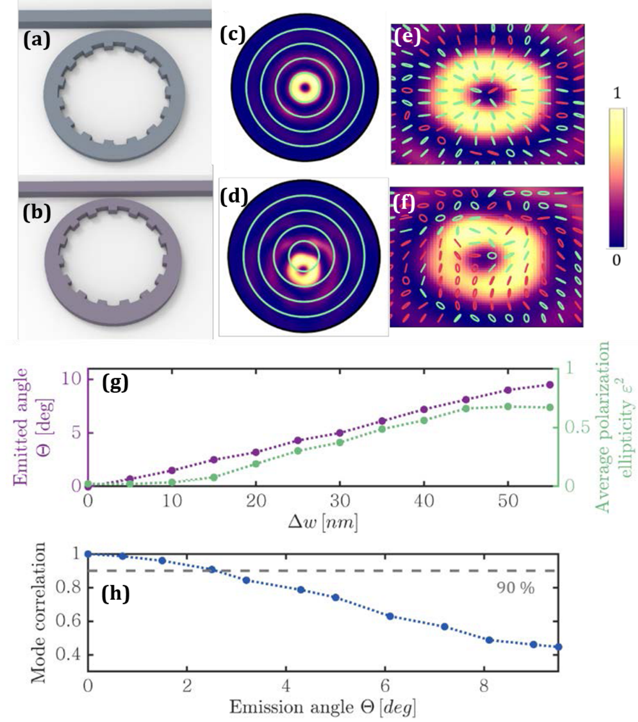

Fig. 2. (a) Sketch of a vertical emitter; (b) slant emitter based on width variation. (c), (d) Far-field intensity emission with each concentric ring (green) representing 10°; (e), (f) polarization map of the $l = 0$ emitted mode for the case of (c), (e) vertical emission and (d), (f) slant emission. (g) Emission angle and average polarization ellipticity of the $l = 0$ mode as afunction of the width change Δw in the microring resonator. (h) Mode correlation as function of the emission angle. The dashed line highlights mode correlation of 90%.

A comparison between the emitted CVV beams with topological phase $l = 0$, without and with superimposed linear phase obtained by the variation of the waveguide width, is presented in Fig. 2. The geometries of the microrings are illustrated in Figs. 2(a) and 2(b). In both cases, the microring radius is 3.9 μm, and the waveguide height is 180 nm. The vertical emitter consists of a constant waveguide width of 450 nm while width of the slanted emitter waveguide varies by $\Delta w = \pm 50$ nm, from 400 nm to 500 nm, along the y coordinate [defined in Fig. 1(a)]. In both cases, 33 equally spaced grating elements are used. Each scatterer consists of a 100 nm wide, 200 nm long, and 180 nm high cuboid. The gap between the bus waveguide and the microring is 50 nm. Figures 2(c) and 2(d) shows the far-field intensity projection of the simulated field, propagated onto a hemispherical surface of 1 m radius. The figure presents the typical "doughnut" shape of CVV beams. The emission angle obtained by tuning the waveguide dimensions is about $\Theta = 9°$.

Figures 2(e) and 2(f) present a map of the polarization of the emitted CCV beams. While the vertically emitted beam is almost perfectly radially polarized, the polarization of the tilted beam is more complex. This is mainly due to the fact that the local polarization scattered by the grating elements varies with the geometry of the waveguide [13]. Although the polarization of CVVs varies in space, the cylindrical average global ellipticity can be used to characterize the average polarization of the mode. The average cylindrical polarization ellipticity is defined as the ratio of the radial and azimuthal energy components of the

CVV mode (i.e., $\varepsilon^2 = |E_r|^2/|E_\phi|^2$ or $|E_\phi|^2/|E_r|^2$) such that $\varepsilon^2 = 0$ is linearly polarized (radially or azimuthally) and $\varepsilon^2 = 1$ is circularly polarized. The average ellipticity of the vertically emitted beam is $\varepsilon^2 = 0.023$ and $\varepsilon^2 = 0.677$ for the case of tilted emission.

The emission angle and the average cylindrical ellipticity as a function of the variation in waveguide width are presented in Fig. 2(g). The parameter Δw represents the relative change from the nominal width of $w_0 = 450$ nm, with waveguide width varying from $w_0 - \Delta w$ to $w_0 + \Delta w$. The figure shows that the emission angle increases monotonically, with the increased variation of the waveguide width, such that the global linear superimposed phase is $\Delta\varphi_w = \frac{2\pi R}{\lambda}\Delta n_{\text{eff}}$, with $\Delta n_{\text{eff}} = n_{\text{eff}}(w_0 + \Delta w) - n_{\text{eff}}(w_0 - \Delta w)$. In parallel, the average cylindrical ellipticity also changes, and the beam polarization is altered. This is mainly due to the fact that the polarization in the evanescent field scattered by the grating elements changes with the waveguide width [13].

Another way to characterize the change in the emitted beam is the mode correlation between the vertically emitted beam and the slant emission. Mode correlation can measure the overall similarity between two vector light fields, including intensity, phase, and polarization [21,22]. It is presented in Fig. 2(h), and as expected, the correlation drops with respect to the emission angle. Up to an emission angle of about 2.5°, the mode correlation is higher than 90%.

In the second approach, the width of the waveguide is kept constant, and the superimposed linear phase is implemented by chirping the angular grating. The accumulated phase between two grating elements is $\Delta\varphi_i = \frac{2\pi n_{\text{eff}} R}{\lambda}\Delta\phi_i$, where $\Delta\phi_i$ is the relative azimuthal distance between the two scatterers.

Mathematically, the angular phase matching condition [Eq. (1)] arises from coupling mode theory, in which the grating is considered as a small perturbation in the dielectric constant of the microring that couples the unperturbed WGM of the ring to free-space modes [9]. This condition can be generalized to $\int_0^{2\pi}(l - p + f(\phi))d\phi = 0$, where $f(\phi)$ is the instantaneous angular frequency of the grating. Because l and p are integers, $f(\phi)$ must fulfill the following condition:

$$\int_0^{2\pi} f(\phi)\, d\phi = 2\pi m, \tag{2}$$

where m is an integer that corresponds to the number of grating elements and should satisfy the relation $m = p - l$.

It is trivial to show that when the instantaneous angular frequency of the grating is constant $f(\phi) = \text{const} = g \cdot q$, with g an integer and $q = 2\pi R/\Lambda_0$, the previous condition is fulfilled.

In order to induce a linear phase shift in one Cartesian direction, we need to find the appropriate function $f(\phi)$. Assuming that additional phase goes from 0 to $\Delta\varphi$ when the y-coordinated varies from 0 to 2 R, the linear phase $\varphi_{\text{lin}}(\phi)$ in cylindrical coordinate system can be written as

$$\varphi_{lin}(\theta) = \Delta\varphi/2R \cdot y(\phi) = \Delta\varphi \cdot \sin^2(\phi/2), \tag{3}$$

where we have expressed the y Cartesian coordinate as $y = 2R\sin^2(\phi/2)$ with $0 \le y \le 2R$, instead of the more trivial case of $y = R\sin(\phi)$, with $-R \le y \le R$, for convenience.

The instantaneous angular frequency can be written as $f(\phi) = a \cdot \varphi_{\text{tot}}(\phi) = a \cdot [\varphi_0 + \varphi_{\text{lin}}(\phi)] = a \cdot [2\pi R/\Lambda_0 + \Delta\varphi \cdot \sin^2(\phi/2)]$, where a is the normalization constant, which fulfill the angular momentum phase matching condition,

$$a = \frac{2\pi\,(p - l)}{\int_0^{2\pi}\varphi(\phi)\, d\phi}. \tag{4}$$

The waveform of the grating is given by $G(\phi) = \cos(F(\phi))$, with $F(\phi) = \int_0^{\phi} f(\theta)d\theta$. For the case of a binary grating, each grating element should be positioned at each cycle of the function $G(\phi)$.

To demonstrate the ability of our design to tune the emission angle of CVV beams, we simulate a silicon microring resonator with a radius of 3.1 µm, a waveguide width of 700 nm, and height of 180 nm. In this case, we kept the number of grating elements to be 31, despite the non-uniform spacing. The gap between the bus waveguide and the ring is 100 nm. The comparison between vertical emission and slant emission, for topological phases $l = -1, 0, 1$, is presented in Fig. 3. For this simulation, the additional phase was $\Delta\varphi = 3\pi/2$, which resulted in an emission angle of about $\Theta = 12°$.

The average cylindrical polarization ellipticity is also affected by the superimposed linear phase. It changes from $\varepsilon_0^2(l = -1) = 0.6304$, $\varepsilon_0^2(l = 0) = 0.3993$, $\varepsilon_0^2(l = 1) = 0.8855$ at vertical emission to $\varepsilon_\Theta^2(l = -1) = 0.4776$, $\varepsilon_\Theta^2(l = 0) = 0.6594$, and $\varepsilon_\Theta^2(l = 1) = 0.7864$ for topological phases of -1, 0, and 1, respectively. The emission angle and

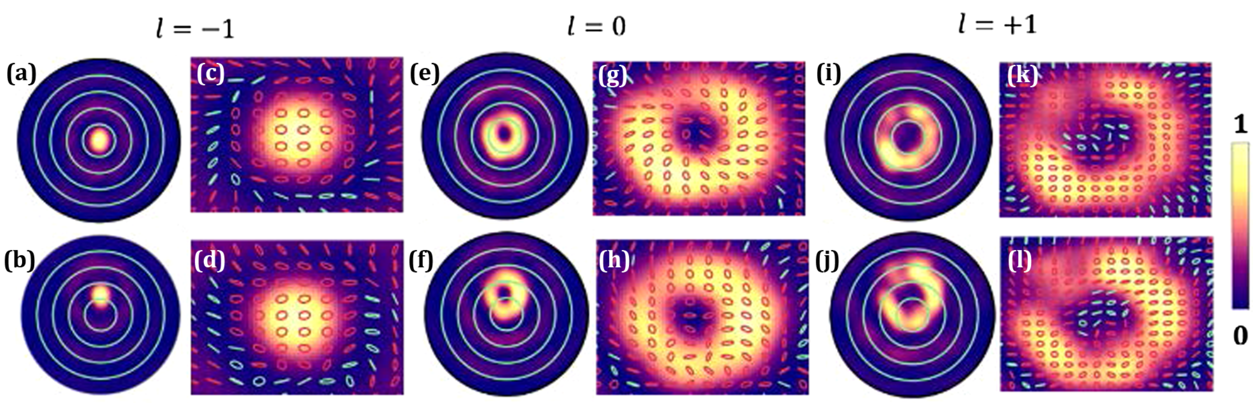

Fig. 3. (a), (b), (e), (f), (i), (j) Far-field intensity emission; (c), (d), (g), (h), (k), (l) polarization map of the emitted modes with topological charge, (a)–(d), $l = -1$; (e)–(h), $l = 0$; (i)–(l), $l = 1$, for the case of (a), (c), (e), (g), (i), (k) vertical emission and (b), (d), (f), (h), (j), (l) slant emission.

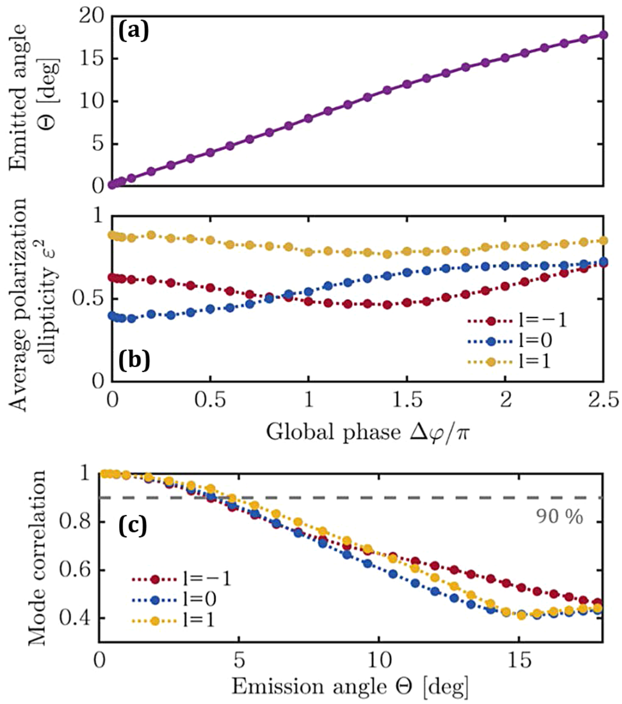

Fig. 4. (a) Emission angle and (b) average cylindrical ellipticity of the CVV modes with topological charges $l = -1, 0, 1$, as a function of the global superimposed phase. (c) Mode correlation as a function of the emission angle. The dashed line represents correlation of 90%.

the average ellipticity as a function of the different superimposed global linear phase $\Delta\varphi$ are presented in Figs. 4(a) and 4(b). The different tendencies with respect to topological charges are not trivial. This change is mainly due to the breaking of cylindrical symmetry, since constructive interference of all the radiating dipole, defined by the local electric field scattered by the grating elements, now occurs at a nonzero angle with respect to the center axis of the ring. However, in this approach, the SoP of the local scattered field is decoupled from the global superimposed phase, such that the ability to tailor the SoP of the CVV beams is maintained. In order to see how the beam quality is affected by the global phase, the mode correlation between the vertical and slant emitted beam as a function of the emission angle is also presented in Fig. 4(c). For an emission angle smaller than $\sim 5^\circ$, the beam is well correlated with the vertical emission, with $>90\%$ correlation.

In conclusion, we have presented two methods to tune the angle of emission from integrated CVV emitters. The first method is based on width variation of the ring's waveguide, which should be relatively easy to implement, however, at the expense of significantly perturbation to the SoP of the emitted beam. The second method is based on a chirped grating, and it keeps the ability to tailor the SoP of the emitted beams by decoupling the superimposed phase from the waveguide geometry.

While the approach discussed here was focused on the linear regime, slanted emission of CVVs could also become an important feature for achieving phase matching in efficient nonlinear processes, which are important building blocks for development of new functionalities for chip-scale quantum technologies. Moreover, the mathematical method presented here is not limited to imprinting a linear phase in a Cartesian coordinate, but it can be also used to apply any phase profile on the ring. For example, more complex CVVs profiles composed of two or more orthogonal modes, as in Ref. [16], can be generated.

Acknowledgment. Y. S. acknowledges a fellowship from Hebrew University center for nanoscience and nanotechnology.

Disclosures. The authors declare no conflicts of interest.

REFERENCES

1. A. F. Abouraddy and K. C. Toussaint, Phys. Rev. Lett. **96**, 153901 (2006).
2. M. Padgett and R. Bowman, Nat. Photonics **5**, 343 (2011).
3. M. P. MacDonald, L. Paterson, K. Volke-Sepulveda, J. Arlt, W. Sibbett, and K. Dholakia, Science **296**, 1101 (2002).
4. V. D'Ambrosio, N. Spagnolo, L. Del Re, S. Slussarenko, Y. Li, L. C. Kwek, L. Marrucci, S. P. Walborn, L. Aolita, and F. Sciarrino, Nat. Commun. **4**, 2432 (2013).
5. J. Wang, J. Y. Yang, I. M. Fazal, N. Ahmed, Y. Yan, H. Huang, Y. Ren, Y. Yue, S. Dolinar, M. Tur, and A. E. Willner, Nat. Photonics **6**, 488 (2012).
6. G. Vallone, V. D'Ambrosio, A. Sponselli, S. Slussarenko, L. Marrucci, F. Sciarrino, and P. Villoresi, Phys. Rev. Lett. **113**, 060503 (2014).
7. J. T. Barreiro, T. C. Wei, and P. G. Kwiat, Phys. Rev. Lett. **105**, 030407 (2010).
8. F. Bouchard, R. Fickler, R. W. Boyd, and E. Karimi, Sci. Adv. **3**, e1601915 (2017).
9. X. Cai, J. Wang, M. J. Strain, B. Johnson-Morris, J. Zhu, M. Sorel, J. L. O'Brien, M. G. Thompson, and S. Yu, Science **338**, 363 (2012).
10. S. A. Schulz, T. Machula, E. Karimi, and R. W. Boyd, Opt. Express **21**, 16130 (2013).
11. J. Liu, S. M. Li, L. Zhu, A. D. Wang, S. Chen, C. Klitis, C. Du, Q. Mo, M. Sorel, S. Y. Yu, X. L. Cai, and J. Wang, Light Sci. Appl. **7**, 17148 (2018).
12. M. J. Strain, X. Cai, J. Wang, J. Zhu, D. B. Phillips, L. Chen, M. Lopez-Garcia, J. L. O'Brien, M. G. Thompson, M. Sorel, and S. Yu, Nat. Commun. **5**, 4856 (2014).
13. Z. Shao, J. Zhu, Y. Chen, Y. Zhang, and S. Yu, Nat. Commun. **9**, 926 (2018).
14. Z. Shao, J. Zhu, Y. Zhang, Y. Chen, and S. Yu, Opt. Lett. **43**, 1263 (2018).
15. J. Zhu, X. Cai, Y. Chen, and S. Yu, Opt. Lett. **38**, 1343 (2013).
16. Q. Xiao, C. Klitis, S. Li, Y. Chen, X. Cai, M. Sorel, and S. Yu, Opt. Express **24**, 3168 (2016).
17. F. Ripka, H. Kübler, R. Löw, and T. Pfau, Science **362**, 446 (2018).
18. G. Walker, A. S. Arnold, and S. Franke-Arnold, Phys. Rev. Lett. **108**, 243601 (2012).
19. L. Stern, R. Zektzer, N. Mazurski, and U. Levy, Laser Photon. Rev. **10**, 1016 (2016).
20. R. Ritter, N. Gruhler, W. H. P. Pernice, H. Kübler, T. Pfau, and R. Löw, New J. Phys. **18**, 103031 (2016).
21. M. W. Beijersbergen, R. P. C. Coerwinkel, M. Kristensen, and J. P. Woerdman, Opt. Commun. **112**, 321 (1994).
22. H. Ma, Y. Zhang, C. Min, and X. Yuan, Opt. Lett. **45**, 4823 (2020).